https://doi.org/10.7735/ksmte.2026.35.1.6

J. Korean Soc. Manuf. Technol. Eng.
ISSN 2508-5107(Online)

Ultrasonic Beam Profile Characteristics for Surface Defect Detection in Mobility Components

Peng Zhang[a], Xiaohan Wu[a], Hao Zhu[a], Gui-Lin Zhang[a], Young-Tae Cho[b], Yun-Taek Yeom[c], Seung-Kug Kim[a,d], Kwang-Hee Im[e,*]

[a] Department of Automotive Engineering, Graduate School of Woosuk University
[b] Department of Basic Science, Jeonju University
[c] Department of Smart Mechanical Engineering, Dongyang University
[d] CV New Vehicle Quality Team, Hyundai Motor Company
[e] Department of Mechanical and Automotive Engineering, Woosuk University

ARTICLE INFO

Article history:
Received 2 January 2026
Revised 11 January 2026
Accepted 12 January 2026

Keywords:
NDE techniques
Defect detection
Mobility components
Beam profile
Ultrasonic waves

ABSTRACT

Nondestructive ultrasonic technology has garnered significant interest from various industries, including agriculture, medical engineering, and airport security. In general, microcracks formed during the machining of mobility components not only degrade performance but also reduce overall quality. Therefore, appropriate nondestructive techniques are required to ensure the reliability of mobility components. Rayleigh waves were utilized for surface monitoring of the mobility parts, and ultrasonic beam radiation measurements were performed to predict beam profile behavior. A contact-type measurement jig was used to measure surface defect reflections. Furthermore, Rayleigh wave generation and optimal testing conditions were realized through CIVA simulation, which provided insights into ultrasonic behavior under controlled conditions.

1. Introduction

Recently to evaluate the physical properties and integrity of mobility components, non-destructive testing (NDT) techniques are employed[1-3]. In particular, when using ultrasonic pulse signals, the time-of-flight (TOF) measurement along the acoustic propagation direction is utilized. By fabricating specimens that allow both-sided inspection, simultaneous measurement of specimen thickness and ultrasonic velocity can be achieved[4-10]. Furthermore, experimental studies have been conducted using SM45C material, which exhibits excellent mechanical properties for automotive components, with micro-scale surface defects introduced for research purposes[11].

Also, for large vessels manufactured domestically, welding defect and coating inspections are performed manually during construction and delivery. However, such manual inspections are inherently incomplete, thereby affecting shipowner confidence. To address this issue, a remotely operated ultrasonic inspection system was developed for underwater and surface applications, enabling automated detection of dissimilar-metal weld defects in ship hull structures. This system allows remote observation and inspection of target areas, and the present study introduces

* Corresponding author. Tel.: +82-63-290-1473
E-mail address: khim@woosuk.ac.kr (Kwang-Hee Im).

its application to artificial defects in aged dissimilar-metal welds[12].

Additionally, a horizontal measurement device of ultrasonic welding tool was proposed, incorporating multiple guide bars to align the ultrasonic welding tool. A corresponding horizontal measurement method was also presented[13].

Presently, domestic efforts are underway to develop NDT techniques tailored for piping systems. Automated ultrasonic inspection systems are widely applied to mechanical components such as tanks and turbine welds in power generation facilities. These systems enable effective inspection while moving across designated areas, and the developed software provides real-time visualization of inspection processes, convenient data storage, on-site interpretation, and direct report generation and printing[14].

For mobility components, ultrasonic contact mode was employed to investigate the influence of ultrasonic beams on surface defects. Reflection signals were analyzed with respect to defect orientation. During ultrasonic experiments, SM45C specimens with machined surface defects were tested using a pitch-catch mode with transducers applied from a single direction. A simplified contact-type system was established to measure Rayleigh wave velocity in mobility components. The system automatically classified signals by channel, loaded them into memory, and displayed inspection data with high speed and accuracy.

To further evaluate ultrasonic characteristics, surface-defect specimens were tested using the pulse-echo method, enabling acquisition of defect signals from both front and back surfaces. Rayleigh wave generation and optimal testing conditions were simulated using CIVA software, which provides insights into ultrasonic behavior. Particularly, under the pitch-catch mode, selecting an ultrasonic amplitude range with a high signal-to-noise ratio from reflection signals demonstrated its potential as a key parameter in NDT evaluations.

2. Ultrasonic System

2.1 Samples

In this experiment, artificial defects were machined on the surface of SM45C material, which is commonly used for mobility components. The specimens were prepared with

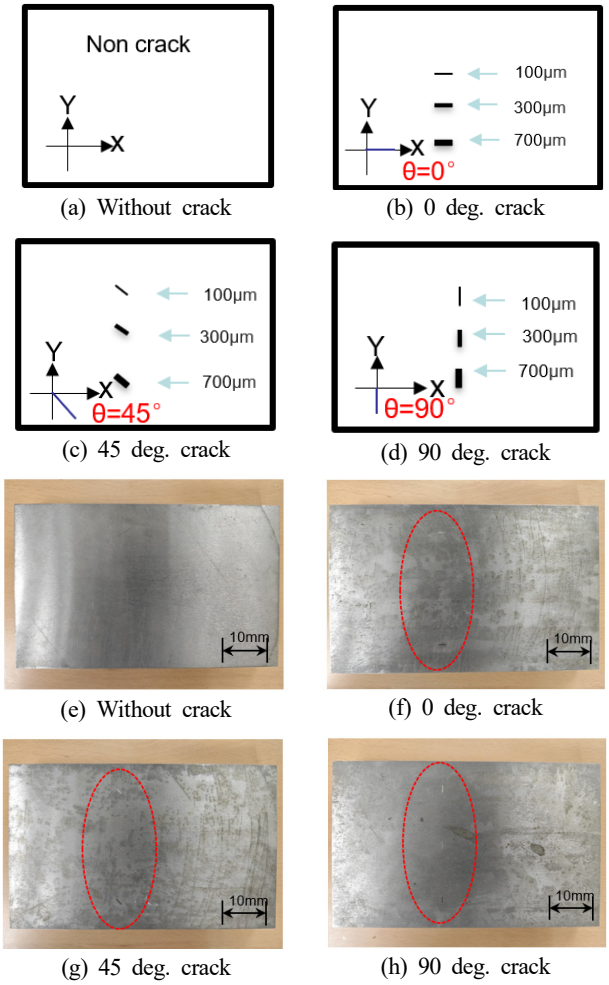

(a) Without crack (b) 0 deg. crack (c) 45 deg. crack (d) 90 deg. crack (e) Without crack (f) 0 deg. crack (g) 45 deg. crack (h) 90 deg. crack

Fig. 1 Sample configuration and micro cracks of ultrasonic experimentation for generating surface waves

defect depths of 0 μm, 100 μm, 300 μm, and 700 μm. Ultrasonic testing was then conducted under four conditions: defect-free, defect orientation at 0°, 45°, and 90°. Fig. 1 illustrates the defect sizes and orientations of the test specimens.

2.2 Rayleigh wave

In this experiment, as shown in Fig. 2, a surface wave (Rayleigh wave) is generated at the liquid-solid interface when the incident ultrasonic wave reaches the Rayleigh angle. At this angle, all ultrasonic energy is converted into Rayleigh surface waves that propagate along the surface. The Rayleigh wave is defined as a type of surface wave in which the energy is concentrated and transmitted along the solid surface[1].

Furthermore, the principle of surface wave generation is derived by applying Snell's law, as expressed in

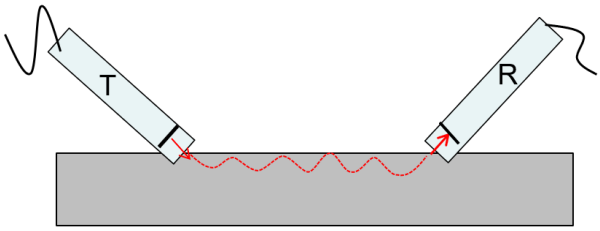

Fig. 2 Ultrasonic experimentation for generating surface waves in UT system

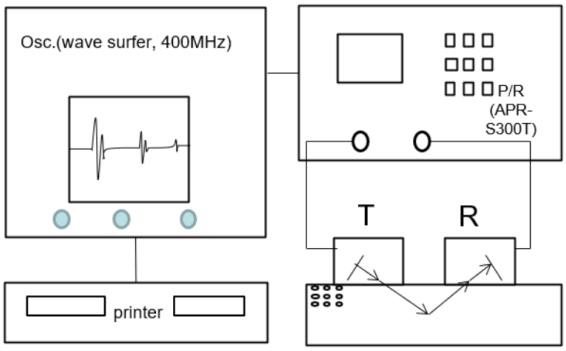

Fig. 3 Ultrasonic schematic diagram of ultrasonic testing setup

Equation (1)[1].

$$\frac{\sin\theta 1}{\sin\theta 2}=\frac{\sin\theta'}{\sin\theta 2}=\frac{\sin\theta''}{\sin\theta 3}\frac{V_1}{V_2} \quad (1)$$

Here, V_1 and V_2 denote the ultrasonic velocities in the medium and steel, respectively. As shown in Fig. 2, when an ultrasonic wave is incident on the specimen, both longitudinal and transverse waves are generated. By determining the critical angle of the transverse wave and directing it to the surface, a surface wave is produced.

2.3 Experimental apparatus

Fig. 3 presents the schematic of the ultrasonic testing apparatus, illustrating the overall experimental setup. The testing method employed a direct Rayleigh ultrasonic probe, with ultrasonic waves generated using an APR-S300T PR spike voltage pulser/receiver (AIQS). The RF waveforms produced by the test specimens were acquired using an oscilloscope (Wave Surfer 42Xs-A) and subsequently stored on a computer. Multiple echo signals displayed on the oscilloscope could be independently shifted, stored, and compared, enabling convenient measurement and analysis. In this experiment, to maximize the ultrasonic signal, a

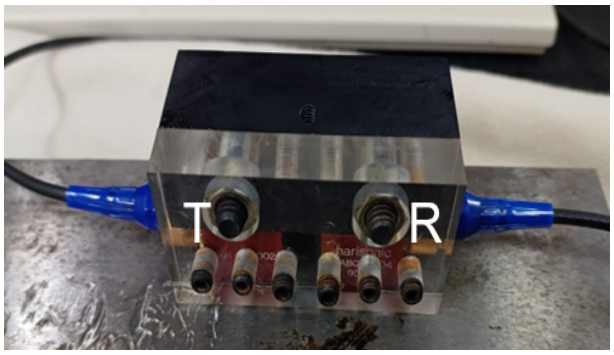

Fig. 4 Ultrasonic wave transducers for generating Rayleigh wave

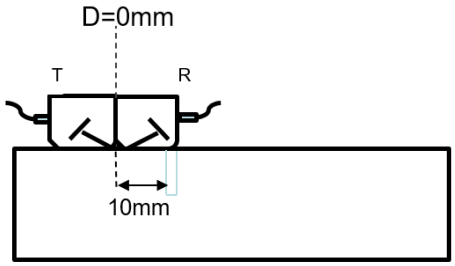

(a) In case of 0 mm of probe separation distance (D) with no defect

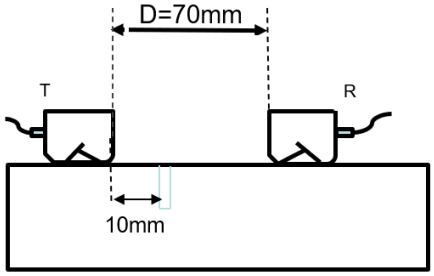

(b) In case of 70 mm of probe separation distance (D) with a defect

Fig. 5 One-sided measurement method on the sample

Rayleigh ultrasonic probe consisting of two transducers was employed.

A low frequency of 2.25 MHz—appropriate for surface cracks—was selected. Fig. 4 illustrates the two probes used in the experiment, both of which are 2.25 MHz Rayleigh ultrasonic probes (90° ST) manufactured by Harisonic Co.

2.4 Experimental method

The ultrasonic testing setup consisted of a digital storage oscilloscope (DSO; Lecory, Wave Surfer) for digitizing ultrasonic signals and enabling PC-based data exchange, a pulse-echo receiver (AIQS, APR-S300T) capable of transmitting and receiving at 250,000 bits per second over distances up to 1000 m, and a Rayleigh ultrasonic probe

serving as the transducer. Specifically, Fig. 5(a) represents the case where D = 0 mm, while Fig. 5(b) illustrates the measurement method for D = 70 mm. Fig. 5 depicts the measurement of ultrasonic signals during the ultrasonic testing. The transmitting transducer (T) was fixed, and the receiving transducer (R) was moved to acquire the signals. Ultrasonic testing was performed at every 2 mm interval from D = 0 mm to D = 70 mm. Furthermore, a contact-type jig was implemented, and a simplified automated system was developed in LabVIEW for signal acquisition and processing.

3. Ultrasonic Simulation

In Section 3, a 2.25 MHz ultrasonic transducer was employed to detect defects in samples of SM45C plates designed for mobility applications. To assess the surface cracks of the samples, pitch-catch ultrasonic beam measurements were conducted at the different depth cracks relative to the crack orientation reference (0°). Identifying the effective parameters for ultrasonic testing under these directional conditions is critical. Accordingly, the NDE CIVA package (CIVA 2025, NDE CIVA) was utilized to establish optimal ultrasonic simulation conditions.

In this simulation, ultrasonic behavior was modeled as illustrated in Figs. 6-7. The ultrasonic transducers were positioned on the surface of the test specimen and configured using the pitch-catch method. Fig. 6 shows the pitch-catch.

3.1 Ultrasonic simulation setup

Technique with two ultrasonic transducers separated by 10 mm, applied to a sample of SM45C plates without defects.

The corresponding received ultrasonic signal is presented as an A-scan on the left. Fig. 8 depicts the case of a samples of SM45C plates containing a defect, again employing the pitch-catch method with the 24 mm probe separation. The received signal is likewise displayed as an A-scan on the left.

Analysis of the A-scan data revealed a considerable number of reflected signals, indicating that both defects and crack orientations in the sample of SM45C plates influenced the results. To evaluate the ultrasonic beam characteristics of the samples of SM45C plates, the ultrasonic simulation further modeled pitch-catch beam profiles at 0°, 45°, and 90° relative to the crack orientation.

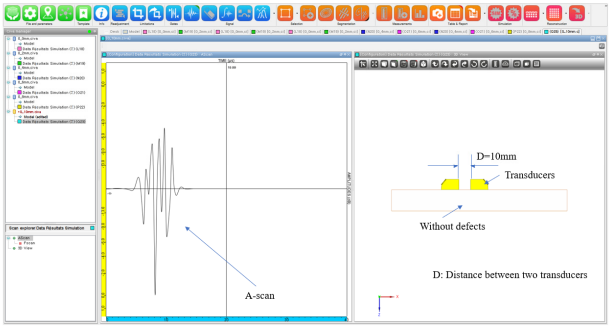

Fig. 6 Pitch-catch mode set up for two ultrasonic transducers at the distance of 10 mm without defects

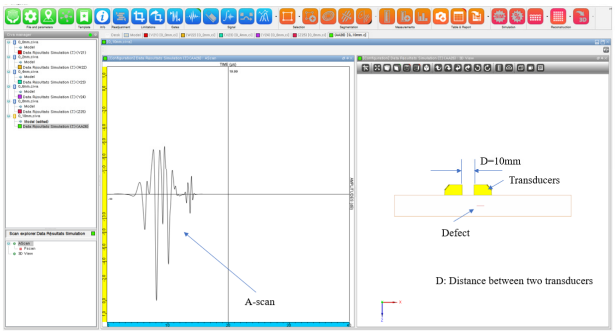

Fig. 7 Pitch-catch mode set up for two ultrasonic transducers at the distance of 24 mm with defects

4. Results and Discussion

4.1 Ultrasonic simulation

The ultrasonic testing was simulated using the pitch-catch mode. In this simulation, the ultrasonic frequency was set to 2.25 MHz, and the transducer dimensions were 18 × 16 × 8.4 mm. It was assumed that a 100 μm defect was machined on the surface of SM45C steel, and ultrasonic waves were generated in pitch-catch mode.

Fig. 8(a) shows the case without surface defects, where the simulation produced Rayleigh waves with large amplitudes on the specimen surface, resulting in strong received ultrasonic signals. In contrast, Fig. 8(b) illustrates the case with a 100 μm surface defect. Although Rayleigh waves were excited, the amplitude of reflected signals from the defect was significantly reduced from the received ultrasonic waves, which leadsto relatively weaker signals. It was found this reduction is attributed to the obstruction of the ultrasonic propagation path by the surface defect.

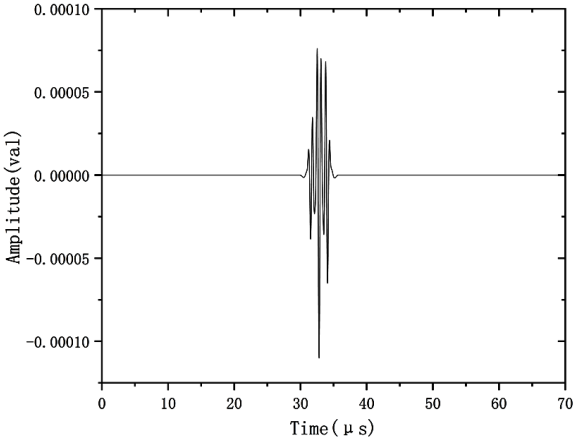

(a) Peak-to-peak amplitude without defects (2.25MHz)

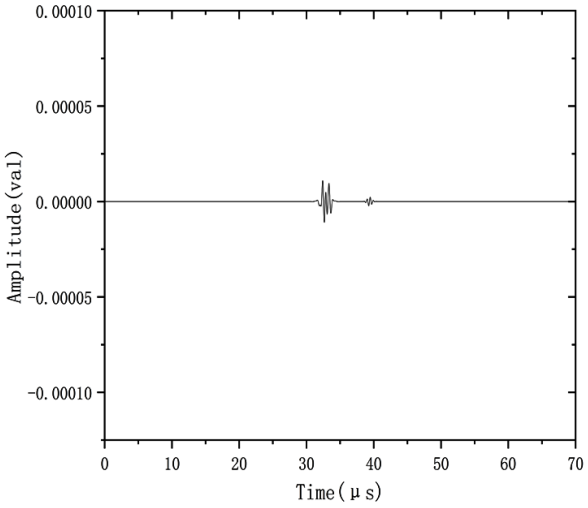

(b) Peak-to-peak amplitude with 100 μm crack (2.25MHz)

Fig. 8 Simulation comparison between with defect and without defect in pitch-catch ultrasonic techniques

4.2 Ultrasonic experimental analysis

As shown in Fig. 9, Rayleigh ultrasonic transducers were applied to a sample of SM45C plates, with the probes oriented at the angles 0 deg. 45 deg. and 90 deg to the crack direction, thereby implementing the pitch-catch mode. In particular, Fig. 7 presents the ultrasonic signal amplitude obtained from the pitch-catch mode of a sample of SM45C plates. In this case, one distinct peak signal is typically observed, for which both the time-of-flight (TOF) and amplitude were measured. Furthermore, by adjusting the probe separation distance between the two ultrasonic transducers, TOF and amplitude were continuously recorded to evaluate the signal behavior.

4.3 Ultrasonic experimental behavior

4.3.1 Crack analysis of pitch-catch mode

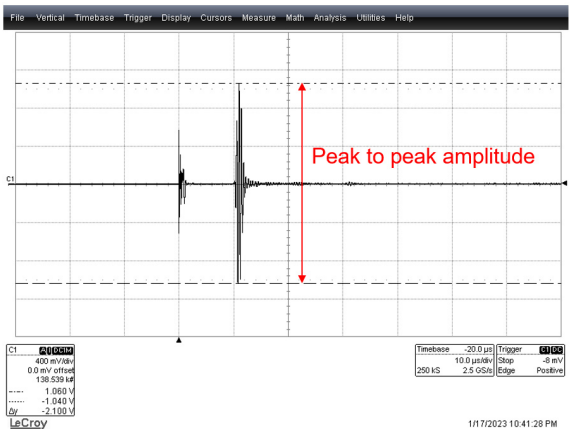

Fig. 9 Ultrasonic signal of Rayleigh wave transducers based on one-sided pitch-catch mode

As shown in Fig. 10, the X-axis represents the location of the probe relative to the defect, while the Y-axis denotes the normalized amplitude. The symbols indicate different defect conditions: "■"represents non-crack, "●"represents 100 μm depth defect, "▲"repersents 300 μm depth defect and "▼" represents 700 μm depth defect on samples. Fig. 10 illustrates the effect of defect depth on the amplitude of ultrasonic waves. As defect depth increases, the reduction in amplitude becomes progressively more pronounced. The most significant variation in amplitude due to defects is observed between 10 mm and 20 mm from the defect's starting position. Different colors are used to distinguish defect depths: red for 100 μm, blue for 300 μm, and green for 700 μm. Fig. 10(a) presents amplitude values for a 0° defect orientation. The curves vary with probe position, showing that as the probe distance increases, the amplitude of Rayleigh waves gradually decreases and their intensity weakens. The red curve (100 μm defect) remains close to the defect-free amplitude, indicating minimal attenuation. In contrast, the green curve (700 μm defect) exhibits a substantial reduction in amplitude, demonstrating that under a 0° defect orientation, Rayleigh wave amplitude decreases both with increasing probe distance and with increasing defect depth. Fig. 10(b) and Fig. 10(c) were confirmed that the same trend observed in Fig. 10(a): the amplitude of Rayleigh waves decreases as probe distance increases, and the magnitude of reduction grows with defect depth. Furthermore, the results indicate that, in addition to depth, different defect types exert varying influences on Rayleigh wave amplitude.

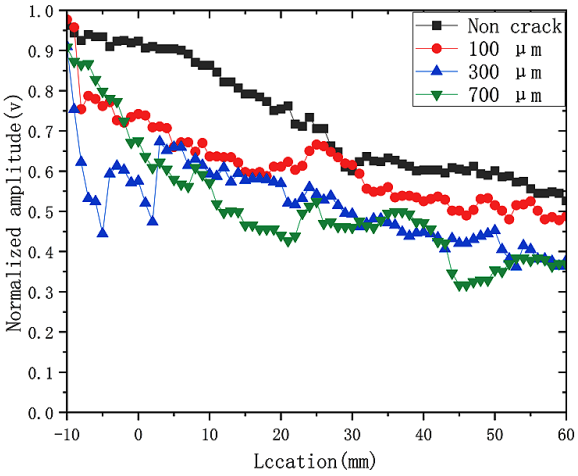

(a) Relationship between normalized amplitude and location of Rayleigh wave transducers with crack in 0° direction for plates

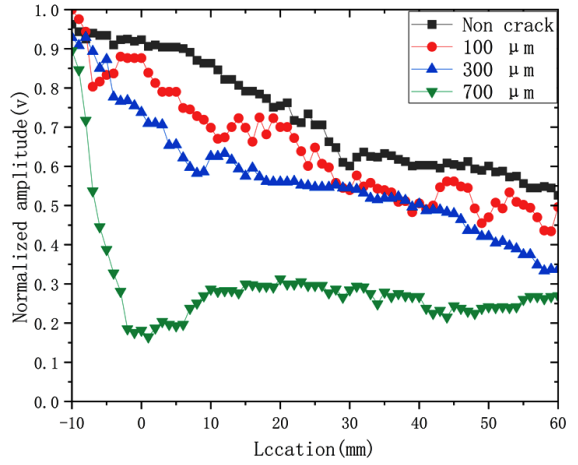

(b) Relationship between normalized amplitude and location of Rayleigh wave transducers with crack in 45° direction for plates

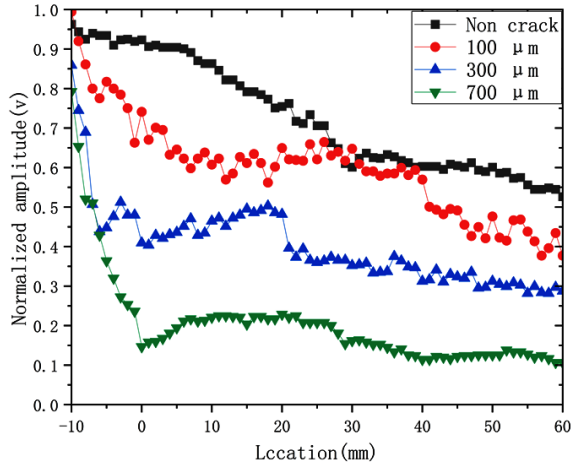

(c) Relationship between normalized amplitude and location of Rayleigh wave transducers with crack in 90° direction for plates

Fig. 10 Relationship between normalized amplitude and location of Rayleigh wave transducers with direction of the same type for plates

4.3.2 Angle analysis of pitch-catch mode

As shown in Fig. 11, the X-axis represents the location of the probe relative to the defect, while the Y-axis denotes the normalized amplitude. The symbols indicate different defect conditions: "■"represents non-crack, "●"represents 0-degree defect, "▲"represents 45-degree defect and "▼"represents 90-degree defect on samples. Fig. 11 illustrates the influence of defect orientation on the amplitude of Rayleigh waves at the same defect depth, along with the corresponding amplitude variation curves as a function of position.

Fig. 11(a): For a defect depth of 100 μm, the curve shows the variation in Rayleigh wave amplitude after passing through the defect. Three colors are used to distinguish defect orientations: red for 0°, blue for 45°, and green for 90°. Fig. 11(b) and Fig. 11(c): These figures present the impact of different defect orientations on Rayleigh wave propagation when the defect depths are 300 μm and 700 μm, respectively. The results demonstrate that both defect orientation and depth significantly affect the attenuation and amplitude variation of Rayleigh waves.

From Fig. 11, it is evident that different types of material defects exert distinct impacts on the propagation of Rayleigh waves. This effect primarily depends on the orientation of the defect and its relative alignment with the direction of ultrasonic wave beam propagation. When the defect is aligned with the propagation direction of the Rayleigh wave beam (0° orientation), the obstruction to the ultrasonic wave is relatively minor. In this case, Rayleigh waves can propagate more smoothly along the extension of the defect, resulting in reduced scattering and attenuation as the waves pass through.

In contrast, when the defect is oriented perpendicular to the propagation direction (90° orientation), the obstruction is most significant. Here, Rayleigh waves encounter greater resistance at the defect interface, as the defect interrupts the continuous propagation path. Consequently, this orientation leads to pronounced attenuation of the ultrasonic wave beam, producing a lower amplitude signal at the receiver.

Furthermore, the differences in ultrasonic signals caused by the presence of defects are clearly observable. Defects within SM45C plate specimens significantly were influenced to ultrasonic amplitude values. Regions exhibiting substantial amplitude variation can be served as effective parameters for

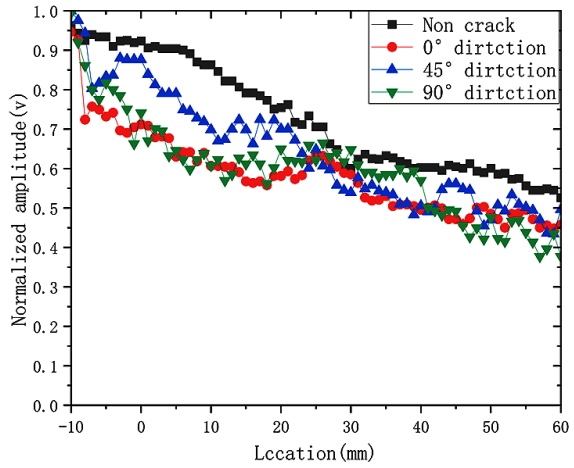

(a) Relationship between normalized amplitude and location of Rayleigh wave transducers with 100 μm deep defect for plates

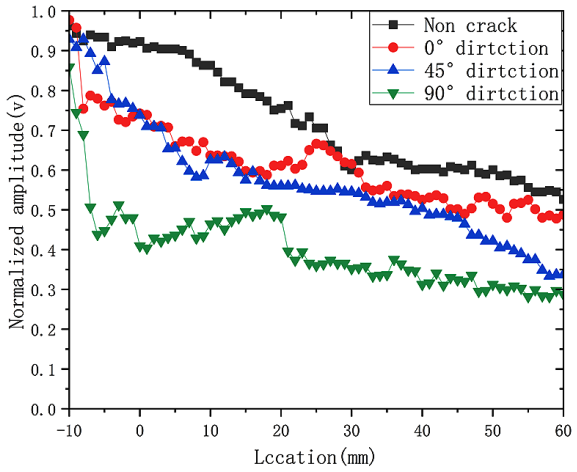

(b) Relationship between normalized amplitude and location of Rayleigh wave transducers with 300 μm deep defect for plates

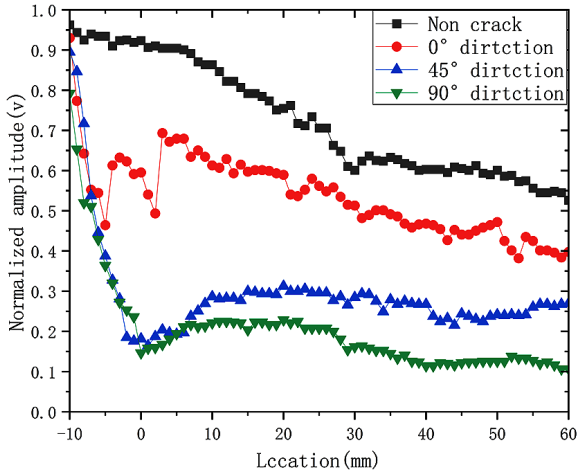

(c) Relationship between normalized amplitude and location of Rayleigh wave transducers with 700 μm deep defect for plates

Fig. 11 Relationship between normalized amplitude and location of Rayleigh wave transducers with same depth defect for plates

C-scan imaging, which provides a high signal-to-noise (S/N) ratio and enhances defect characterization.

5. Conclusions

In this study, to evaluate the surface integrity and characteristics of mobility components, ultrasonic contact mode was employed to investigate the influence of ultrasonic beams on defects. Additionally, the reflection signals corresponding to the orientation of surface defects were analyzed, and Rayleigh wave generation was studied using CIVA simulations to assess ultrasonic behavior. The following conclusions were obtained:

(1) By a sample of SM45C steel plates, direct measurement of time-of-flight (TOF) and amplitude was achieved. A contact-type jig was implemented, and a simplified automated system was developed based on LabVIEW for signal acquisition and processing

(2) Surface defects were machined into the surfce of SM45C steel plates. Ultrasonic testing was performed on the sample tank using a pitch-catch method, successfully acquiring defect signals from the specimen surface..

(3) For defect orientations of 0°, 45°, and 90°, attenuation of Rayleigh waves was most significant when the defect angle was close to 0°. Greater defect depth resulted in stronger attenuation of Rayleigh wave signals.

(4) Assuming machined surface defects, FEM 3D simulations were conducted to generate Rayleigh waves and optimize testing conditions. In the presence of surface defects, the peak-to-peak amplitude was smaller compared to defect-free specimens, indicating that Rayleigh waves propagating along the specimen surface were disturbed by scattering and attenuation.

(5) Since defect angle and depth significantly was to be affected to Rayleigh wave amplitude and TOF, the development of an automated NDE (Non-Destructive Evaluation) system based on FEM simulation is considered necessary.

Acknowledgments

This research was supported by the Regional Innovation

System & Education(RISE) program through the Jeonbuk RISE Center, funded by the Ministry of Education(MOE) and the Jeonbuk State, Republic of Korea.(2025-RISE-13-WSU).

References

[1] Im, K. H., Lee, H. H., Kim, S. K., Jung, J. A., Cho, Y. T., Woo, Y. D., Zhang, Z. L., Kwak, Y. H., Yang, I. Y., 2019, Development of Automatic Ultrasonic System for NDE Characterization on the Heat Treatment in Piston Rods for a Use of Shock Absorbers, J. Korean Soc. Manuf. Technol. Eng., 28:4 238-245, https://doi.org/10.7735/ksmte.2019.28.4.238.

[2] Zhang, G. L., Yeom, Y. T., Kim, S. K., Cho, Y. T., Woo, Y. D., Im, K. H., 2022, Evaluation of NDE Characteristics for Measuring the Painting Thickness in Wind Energy Turbine Power Blades Based on Ultrasonic Wave Simulation, J. Korean Soc. Manuf. Technol. Eng., 31:3 154-161, https://doi.org/10.7735/ksmte.2022.31.3.154.

[3] Liang, H., Shi, X. L., Zhang, P., Zhang, G. L., Yeom, Y. T., Cho, Y. T., Woo, Y. D., Im, K. H., 2023, Characterization on the Beam Profile for Defect Detection of Unidirectional CFRP Composites Using NDE Techniques, J. Korean Soc. Manuf. Technol. Eng., 32:6 326-339, https://doi.org/10.7735/ksmte.2023.32.6.326.

[4] Im, K. H., Lee, K. S., Yang, I. Y., Yang, Y. J., Seo, Y. H., Hsu, D. K., 2013, Advanced T-ray Nondestructive Evaluation of Defects in FRP Solid Composites, Int. J. Precis. Eng. Manuf., 14 1093-1098, https://doi.org/10.1007/s12541-013-0147-2.

[5] Im, K. H., Kim, S. K., Woo, Y. D., Cho, Y. T., Lee, G. S., Yu, B. M., Jung, J. A., Zhang, G. L., 2017, NDE Terahertz Techniques for Measurement of Paint Thickness on Blades for Use in Wind Power, J. Korean Soc. Manuf. Technol. Eng., 26:6 610-616, https://doi.org/10.7735/ksmte.2017.26.6.610.

[6] Jeong, J. A., Hsu, D. K., Im, K. H., 2011, One-sided Nondestructive Evaluation of Back-Side Wedge By using Ultrasonic Sound, J. Korean Soc. Manuf. Technol. Eng., 20:6 773-777.

[7] Goebble, K., 1980, Structure Analysis by Scattered Ultrasonic Radiation in Research Techniques in Nondestructive Testing(ed. Sharpe, R. S.), 4 30-38, Academic Press, London.

[8] Hsu, D. K., Thompson, D. O., Thompson, R. B., 1986, Evaluation of Porosity in Aluminum Alloy Castings by Single-Sided Access, Ultrasonic Backscattering in Review of Progress in Quantitative Nondestructive Evaluation: Volume 5 (ed. Thompson, D. O., Chimenti, D. E.,) 1633-1642, Plenum Press, NY.

[9] Park, H. B., Kim, Y. K., 2019, A Study on Coating Film Thickness Measurement in Vehicle using Eddy Current Coil Sensor, J. Korea Inst. Inf. Commu. Eng., 23:9 1131-1138, https://doi.org/10.6109/jkiice.2019.23.9.1131.

[10] Zhang, X., Augereau, F., Laux, D., Le Clezio, E., Ismaili, N. A., Kuntz, M., Despaux, G., 2014, Non-destructive Testing of Paint Coatings on Steel Plates by Ultrasonic Reflectometry, J. Nondestruct. Eval., 33 504-514, https://doi.org/10.1007/s10921-014-0246-8.

[11] Mezghani, S., Perrin, E., Vrabie, V., Bodnar, J. L., Marthe, J., Cauwe, B., 2016, Evaluation of Paint Coating Thickness Variations based on Pulsed Infrared Thermography Laser Technique, Infrared Phys. Technol., 76 393-401, https://doi.org/10.1016/j.infrared.2016.03.018.

[12] Kim, G. W., Seo. M. K., Choi, N. K., Kim, K. B., Kwon, S. G., Kim, Y. C., 2017, Development of Phased Array Ultrasonic Transducers for Detecting Defects of KR60 Rail Road (I) - Simulation by CIVA Software, J. Korean Soc. Nondestruc. Test., 37:6 411-417, https://doi.org/10.7779/JKSNT.2017.37.6.411.

[13] Jang, H. L., Han, D. H., Kang, L. H., 2020, Thickness Measurement Method of the Paint Coating Layer Using THz-TDS System, J. Korean Soc. Nondestruc. Test., 40:4 259-265, https://doi.org/10.7779/JKSNT.2020.40.4.259.

[14] Shia, X. L., Liang, H., Zhou, Z. H., Zhang, P., Zhang, G. L., Cho, Y. T., Woo, Y. D., Im, K. H., 2023, NDE Techniques of Fiber Characterization in Spar Caps of Wind Turbine Blades using Ultrasonic Waves, J. Korean Soc. Manuf. Technol. Eng., 32:3 119-128, https://doi.org/10.7735/ksmte.2023.32.3.119.

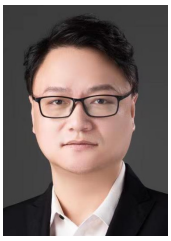

Peng Zhang
Ph.D. candidate in the Department of Automotive Engineering, Graduate School of Woosuk University. His research interests include NDE on composites.
E-mail: 18632959996@163.com

Xiaohan Wu
M.S. candidate in the Department of Automotive Engineering. Graduate School of Woosuk University. Her research interests NDE on materials.
E-mail: wuxiaohan369@gmail.com

Hao Zhu
M.S. candidate in the Department of Automotive Engineering, Graduate School of Woosuk University. His research interests include NDE on material.
E-mail: zhuhao2112@gmail.com

Gui-Lin Zhang
Ph.D. candidate in the Department of Automotive Engineering, Graduate School of Woosuk University. His research interests include NDE on composites.
E-mail: zhengbao1203@naver.com

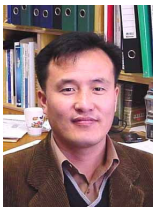

Young-Tae Cho
Associate professor at the Dept. of Basic Science, College of Engineering, Jeonju University. His research interests include nondestructive testing and evaluation of infrared thermography and FEM analysis.
E-mail: dgycho@hanmail.net

Yun-Taek Yeom
Assistant professor in Department of Smart Mechanical Engineering at Dongyang University. His research interests include non-destructive evaluation for material characteristics.
E-mail : ytyeom@dyu.ac.kr

Seung-Kug Kim
Ph.D. candidate in the Department of Automotive Engineering. Graduate School of Woosuk University.
Manager in CV New Vehicle Quality Team, Hyundai Motor Company. His research interests include nondestructive testing and analysis of composite materials for material characteristics.
E-mail : vunctoo@hyundai.com

Kwang-Hee Im
Full professor in Dept. of Automotive Engineering at Woosuk University. His research interests include T-ray/UT nondestructive testing and analysis of composite materials.
E-mail: khim@woosuk.ac.kr